Available online at www.sciencedirect.com
SCIENCE DIRECT
International Journal of Heat and Fluid Flow 27 (2006) 105–122
International Journal of HEAT AND FLUID FLOW
www.elsevier.com/locate/ijhff

Gas/surface heat transfer in spray deposition processes

M. Garbero [a], M. Vanni [b], U. Fritsching [a,*]

[a] Verfahrenstechnik, Universität Bremen, Badgasteiner Straße 3, D-28359 Bremen, Germany
[b] Dip. Scienza dei Materiali e Ingegneria Chimica, Politecnico di Torino, C.so Duca degli Abruzzi 24, 10129 Torino, Italy

Received 4 March 2004; received in revised form 12 January 2005; accepted 5 April 2005
Available online 8 June 2005

Abstract

A numerical investigation of heat transfer dynamics between gas and solid surfaces during droplet spray impingement is presented. Aim of the work is to derive knowledge for control of spray deposition processes like spray painting or spray forming, analysing how the heat exchanged from the surface to the flowing gas is affected by the presence of impinging droplets.

The investigation is carried on a macro- and a micro-scale, analysing velocity and temperature profiles close to a surface cooled by a spray on a scale of the whole spray and on a scale comparable to the droplet diameter, respectively. In the former case an Euler–Lagrange approach is used to reproduce the multiphase jet/spray for different nozzle geometries, gas conditions and droplets properties, as drop diameter and concentration. In the latter case, the gas flow close to the surface is studied during the collision of single and multiple droplets for different impact velocities superposed by different perpendicular gas boundary layer configurations. The "volume of fluid" (VOF) technique is utilized for the determination of the transient shape of the gas–liquid interface during droplet impact. From the data of the numerical case studies, a quantitative consideration about the global increase of surface/gas heat transfer in impinging dilute sprays as a function of the number flux of particles approaching the wall is derived.

Keywords: CFD; Simulation; Drop impact; Spray impingement; Heat transfer

1. Introduction

Impinging sprays are utilized for cooling and/or coating of solid surfaces and preforms. In spray cooling, e.g., for glass tempering or metallic specimen quenching applications, the main portion of the heat from the hot solid surface where the spray impinges is transferred to the liquid droplets or the liquid film on the surface. Within spray quenching, several investigations have derived correlations for the heat transfer coefficient in different flow regimes, depending on atomizer type, spray conditions, and surface conditions. Among them for example Brimacombe et al. (1980), Bolle and Moureau (1982), Mudawar and Valentine (1989), Choi and Yao (1987), Viskanta and Incropera (1992), and Choi and Kang (1993) summarized the results of previous studies for steady-state and transient conditions in liquid- and spray-jets. In spray coating applications, heat transfer between impinging droplets and surfaces has been studied in several studies, e.g., by Armster et al. (2002), Pasandideh-Fard et al. (2001, 2002), Haferl and Poulikakos (2002), and Butty et al. (2002). In these investigations, the liquid/surface heat transfer is by orders of magnitudes larger than the gas/surface heat transfer.

However, especially in processes where the impinging droplets have more or less the same temperature as the underlying solid surface, the total heat flux from the wall may be governed by the heat transfer from the solid surface to the gas in the spray. Prediction of gas/solid heat transfer in impinging sprays has attracted special attention connected with the development of new spray applications such as spray forming of metallic preforms,

* Corresponding author. Tel.: +49 421 218 3663; fax: +49 421 218 7011.
E-mail address: ufri@iwt.uni-bremen.de (U. Fritsching).

0142-727X/$ - see front matter © 2005 Elsevier Inc. All rights reserved.
doi:10.1016/j.ijheatfluidflow.2005.04.003

Nomenclature

a, b	coefficients
B	correlation parameter
C_d	drop concentration
c_p	specific heat capacity
D	jet/nozzle diameter
d	droplet diameter
h	heat transfer coefficient
$\widehat{H}$	total enthalpy
H	nozzle to surface distance
k	conductivity
K	droplet splashing criterion
n	number of droplets
$\dot{n}_p$	number flux of droplets
Nu	Nusselt number, hD/k
Oh	Ohnesorge number $\mu/(\rho d\sigma)^{0.5}$
Pr	Prandtl number
$\dot{q}_w$	wall heat flux
r	radius
R_D	surface roughness
Re	gas Reynolds number, $\rho DU/\mu$
Re_p	particle Reynolds number, $\rho dU_p/\mu$
t	time
T	temperature
T_w	wall temperature
T_f	fluid temperature
$\vec{u}$	gas velocity (vector)
U_g	gas velocity (scalar)
U_p	droplet velocity
We	Weber number, $\rho dU_p^2/\sigma$
x, y, z	coordinates
y_i	mass fraction of species i
Greeks	
α	liquid volume fraction
ω	mass loading
μ	viscosity
ρ	density
τ	dimensionless time, tU_p/d
σ	surface tension

spray painting, and metallization coatings, e.g., for micro-electronic components. The physical phenomena controlling the deposition process are of great importance for the improvement of these applications. Here, typically the properties and characteristics of the sprayed product or coating are in focus of process control investigations. However, theoretical knowledge is difficult to be achieved due to the large amount of strictly connected parameters that have to be analysed.

Numerical investigation of spray processes is an important tool for the analysis and understanding of the governing phenomena since it can give useful information about the local temperature, velocity and pressure fields, which are not easily accessible in experiments due to the simultaneously small time and spatial scales of the phenomena of interest.

In order to achieve accurate predictions of the resulting deposit morphology and micro-structure within spray impingement, it is essential to understand the fluid dynamics of the gas and of the droplets during both their flight towards the surface and their impact phase, as well as heat and mass transfer between droplets, gas and surface.

As an important parameter, the heat transfer coefficient between gas and solid surface in two-phase flow applications is in the focus of the present investigation. In two-phase impinging jets with solid particles, Yokomine et al. (2002) and Sun and Chen (1998) studied the global effect of the presence of the particles in the flow onto the heat transfer. In these studies the solid particles are impacting and rebouncing from the surface, thereby altering the gas flow field in the vicinity of the wall. Based on these studies, in the present contribution the dynamics of the gas/surface heat transfer during droplet spray impact will be analyzed. Here, the effect of depositing liquid droplets on the gas flow field and the resulting gas/wall heat transfer mechanism is in focus. The effect of depositing droplets in a spray is studied from a micro- and macro-modelling point of view. On the macro-scale, the interaction between particle trajectories and gas flow has been considered for an impinging gas/particle (two-phase) jet without particle rebounce. The heat transfer coefficient is calculated with and without particles for different particle loadings, jet velocities, nozzle diameters, and nozzle to wall distances. The Euler–Lagrange approach for dispersed two-phase flow simulations has been adopted for this case.

While the macro-scale analysis concerns the effects on the flow field at the scale of the gas–solid boundary layer thickness, the micro-scale analysis investigates the disturbances originated by each droplet on the gas temperature and velocity profiles at the spatial scale of the droplet. A fully developed boundary layer profile has been assumed as the undisturbed boundary condition for the gas and the liquid spread on to a smooth surface has been simulated for single and multiple droplet impacts and for different droplet and gas velocities. The numerical analysis has been performed by means of a VOF (volume of fluid) method.

From the derived results of the combined macro- and micro-scale simulations, a global estimation of the gas/solid heat transfer increase due to the droplets in the spray has been achieved.

2. Macro-scale analysis

2.1. Modelling of the jet

The impinging jet of gas and droplets has been simulated based on the Euler–Lagrange approach using the CFD code FLUENT. The prediction of the gas flow has been obtained by solving the RANS-equations (see Launder and Spalding, 1974), coupled with an appropriate model for turbulence. Results from different closure models (standard k–ε, k–ω, realizable k–ε, RNG k–ε) have been compared to literature data for the single-phase jet flow from a round nozzle in a quiescent gaseous environment. Among all turbulence model adopted, the best result have been obtained by the realizable k–ε (Shih et al., 1995) and by the RNG k–ε model (Yakhot and Orszag, 1986). The RNG model has shown better prediction of the velocity decay, while the realizable model showed better estimation of the global shape of the jet, where finally the RNG k–ε model has been chosen (Garbero, 2004). For accurate prediction of gas velocity and thermal profiles near the wall, a wall treatment method that combines a two-layer model (Chen and Patel, 1988) with enhanced wall functions (Kader, 1993) has been used.

The dispersed phase is treated by the Lagrangian approach, where a large number of droplet parcels, representing a number of real droplets with the same properties, are traced through the flow field. The representation of droplets by parcels makes it possible to consider the particle size distribution and to simulate the measured liquid mass flow rate at the injection locations by a reasonable number of computational droplets. The trajectory of each droplet parcel is calculated solving the equation of motion for a single droplet (Crowe et al., 1997) neglecting the forces due to virtual mass and history terms. In the spray process, the droplets are considered as spherical and the standard drag correlation for solid spherical particles is used. In order to model the droplet dispersion in the turbulent flow and to obtain a representation of the local velocity, the eddy lifetime concept is applied (Crowe et al., 1997) where the droplet interacts with a sequence of gas eddies with randomly sampled fluctuations.

As a boundary condition during particle impact, the particles are assumed as sticking on the wall in any case. No rebouncing is assumed in order to simulate the case of a completely depositing spray impact.

The steady-state solution of the flow field for both phases is obtained by an iterative calculation. Initially a solution of the gas field is computed without considering the dispersed phase. Afterwards, a large number of discrete parcels are tracked through the flow field and averaged values of momentum source terms for the continuous phase are calculated, see Rüger et al. (2000). At this point, the gas flow field is recalculated considering the influence of droplets by means of the source terms just computed. Then the discrete phase trajectories are calculated again in the modified continuous phase flow field and new source terms are obtained. These steps are repeated until convergence is achieved.

Considering the axial symmetry of the jet, 2D configurations have been used and a mesh with a total number of about 20,000 cells has been adopted. The mesh configuration has been tested to be sufficient to provide grid independent solutions. The regions close to the spray centreline and at the impinged surface have been locally refined for enhanced resolution. This refinement is necessary when the two-layer model is solved with the enhanced wall functions. Even if the enhanced wall treatment is designed to extend the validity of near-wall modelling beyond the viscous sublayer, a mesh that will fully resolve the viscosity-affected near-wall region is recommended. For this reason a sub-grid with at least 10 cells within the viscosity-affected near-wall region ($Re^{+} < 200$) has been generated to be able to resolve the mean velocity and turbulent quantities in that region.

2.2. Results for the macro-modelling

A gas flow exiting a circular nozzle (as in Fig. 1) of diameter D with an average velocity U and cooling a flat surface at a distance H from the nozzle has been considered. The droplets in the jet are assumed to have the same temperature as the impacting surface/wall because here only the gas/wall heat transfer is studied and the heat transfer due to the droplet liquid should not be

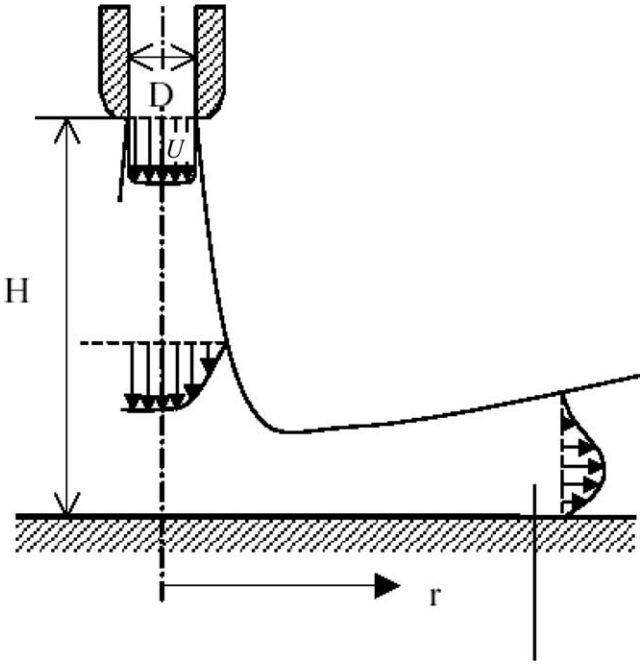

Fig. 1. Impinging jet configuration.

considered by definition. In order to keep the analysis as simple as possible in terms of boundary conditions, the effect of variable gas properties (as density, conductivity, etc.), changing, e.g., with gas temperature has been neglected. Therefore, a rather small temperature difference between gas and droplets/wall of 20 K has been selected. The effect to be studied in this investigation is not changed in this way, because the heat transfer coefficient (or Nusselt number) does not depend on temperature difference, but only on gas flow behaviour and geometry.

The integral averaged Nusselt number within a circular area at different values of the radius has been calculated for the case of gas flow without particles and for different droplet loadings ω (mass flow ratio of droplets to gas).

The particle size distribution is assumed as Rosin–Rammler type distribution, with different mean particle diameters and a constant span value of 2.11. The parameter settings are summarized in Table 1. A number of combinations of these parameters has been performed in the simulation runs. Comparison with the heat transfer coefficient correlation of Schlünder and Gnielinski (as cited in: Verein Deutscher Ingenieure (2002)) has been done for the case of the impinging gas jet without droplets.

Fig. 2(a) shows good agreement between simulations and correlation for the single-phase jet. An increase of the Nusselt number is to be observed due to the macroscopic change of the jet structure by means of the particles in the core region of the jet. All curves of this figure have a maximum on the centreline of the jet. Introducing particles, the inertia of droplets affects the gas flow increasing the heat flux. The effect of the particles is restricted to a small area within a radius $r/D \approx 1$ near the core of the spray, where the droplets impact the surface. In the remaining part of the surface no droplets are found since a condition of trapping at the wall has been assumed for the impinging droplets and therefore the heat transfer does not change significantly in this area.

Table 1
Test cases of jet simulations

$U_{g,0} = U_{p,0}$ [m/s]	10/20/50
H/D [–]	5/10/20
D [mm]	2.5/5/10
ω [–]	0/0.5/1/2
d [μm]	25/50/100/200
Drop number concentration C_d [m^{-3}]	$2.29\times10^5/4.58\times10^5/9.17\times10^5/2.29\times10^6/3.67\times10^6$

The increase of jet inertia is well represented in Fig. 2(b). As it can be seen, the velocity on the centreline of the spray increases by increasing the number of particles in the spray. The impact surface in this case is located in a distance of 0.1 m from the nozzle.

Fig. 3 regards the influence of the jet velocity on heat transfer. The heat transfer at the surface increases with the gas velocity. Actually when the gas velocity is in the range from 10 m/s to 50 m/s, the Nusselt number appears proportional to $U^{0.8}$, provided that drop diameter and mass loading are kept constant. The relationship is confirmed by the work of Huang and El-Genk (1994), who investigated experimentally the heat transfer dynamics of an unconfined jet impinging on a flat plate at low Reynolds numbers and found that the average Nusselt number was proportional to $Re^{0.76}$. This result has been also observed for high mass loadings. The droplet number concentrations for the cases relative to jet velocities of 10 m/s, 20 m/s and 50 m/s are 4.58×10^5, 9.17×10^5 and 2.29×10^6, respectively. The unloaded (pure gas flow) jet result for heat transfer is indicated by the solid symbols in Fig. 3(a). For increasing droplet diameters the behaviour of the two-phase jet approaches the single-phase jet case.

In another series of simulations, the droplet number flux has been kept constant (therefore the loading is changed) while all other boundary conditions are not changed compared to Fig. 3(a). From this result in Fig. 3(b) it can be observed that the gas/surface heat transfer is directly proportional to the droplet diameter

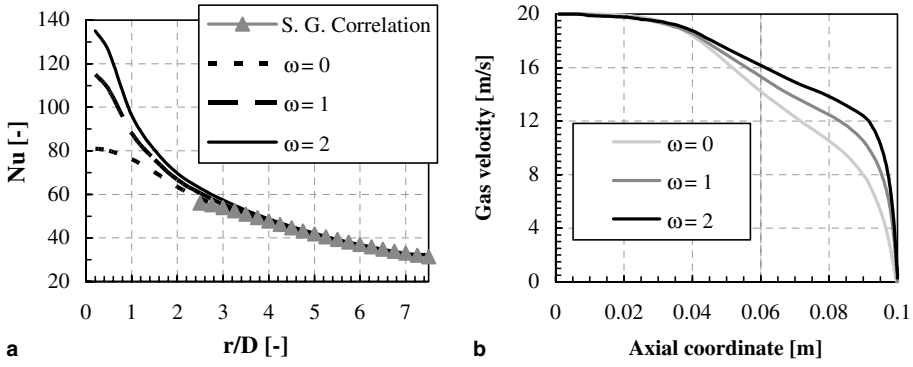

Fig. 2. (a) Integral average of Nusselt number as a function of dimensionless radius and (b) gas velocity decay along the spray axis for an impinging jet with and without droplets; S.G. = data from Schlünder and Gnielinski (as cited in: Verein Deutscher Ingenieure (2002)).

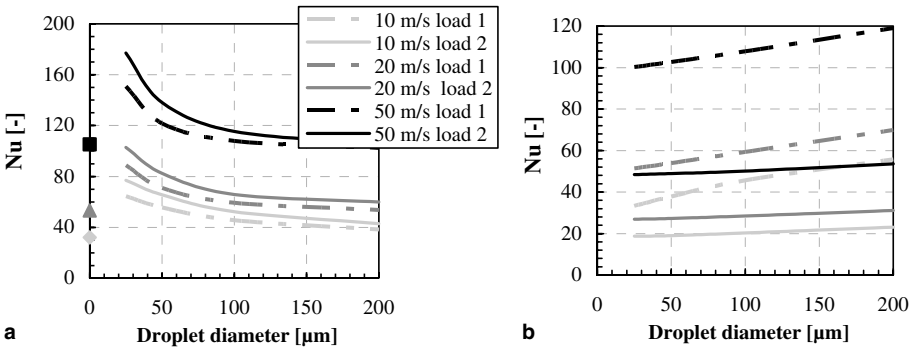

Fig. 3. Influence of jet velocity on the integral Nusselt number as a function of droplet diameter. (a) For different mass loading over a surface of $r/D = 1$. Symbols indicate jet without particles. (b) For constant drop concentration over a surface of $r/D = 1$ (dotted lines) and $r/D = 5$ (continuous lines).

for constant droplet concentration and it shows only a small increase for the surface area of $r/D = 5$. The range of drop diameter considered, from 25 μm to 200 μm, corresponds to a significant variation of diameter in typical spray applications. This means that the influence of the particle diameter for gas heat transfer is not well pronounced. The gas/surface heat transfer mostly depends on the number flux of particles in the spray rather than on their diameter or particle mass loading.

In Fig. 4, the Nusselt number distributions for different nozzle diameters are shown. For a surface area of $r/D = 1$, the variation of the Nusselt number is ambiguous. Obviously, the heat transfer increases with the nozzle diameter since a greater amount of gas is pushed towards the surface. Nevertheless, when comparing the increase of Nusselt number far from the jet, the influence of the nozzle diameter seems equal to that of gas velocity. This behaviour is confirmed by Holloworth and Gero (1985), who analysed the diameter dependency on heat transfer for a jet impinging on a isothermal plate, concluding that the jet diameter has no effect on the Nusselt number for $H/D > 10$. However, some authors as San et al. (1994) have also found that, for the same Reynolds number, smaller jet diameters result in lower values of Nusselt numbers.

Regarding the presence of droplets, in this case, the increase of the integral Nusselt number seems to be more pronounced for smaller diameters, but at smaller areas considered. For the curves relative to $r/D = 5$ of Fig. 4(b), relatively to a constant number flux of particles, the same consideration done before about the velocity influence can be done.

When increasing the distance between wall and nozzle, the heat transfer decreases (Fig. 5) because of the jet velocity decay that results in a reduction of the impingement velocity close to the surface as well as in lower turbulence intensity in the flow field. From the figure it appears that for higher distances the curves of the integral Nusselt number have a different behaviour. Here the spray cone widely spreads and the droplets cover a larger surface area. Actually the spray for the case of 25 μm droplets impinges on a surface area larger than $r/D = 1$. Considering a larger area, from $r/D = 1$ to $r/D = 5$, the behaviour of the heat transfer increment becomes almost the same for all the curves, as is to be seen in Fig. 5(b).

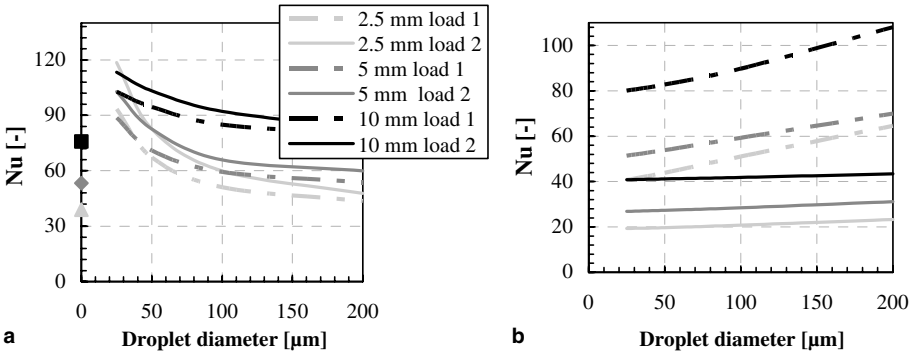

Fig. 4. Influence of nozzle diameter on the integral Nusselt number as a function of droplet diameter. (a) For different mass loading over a surface of $r/D = 1$. Symbols indicate jet without particles. (b) For constant drop concentration over a surface of $r/D = 1$ (dotted lines) and $r/D = 5$ (continuous lines).

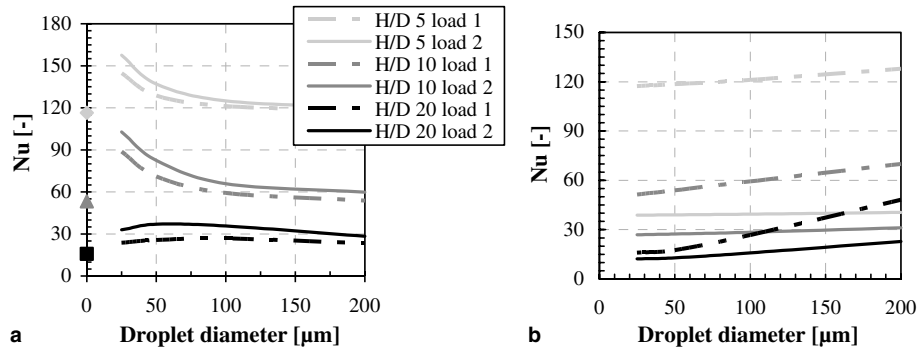

Fig. 5. Influence of wall/nozzle distance on the integral Nusselt number as a function of droplet diameter. Symbols indicate jet without particles. (a) For different mass loading over a surface of $r/D = 1$. (b) For constant drop concentration over a surface of $r/D = 1$ (dotted lines) and $r/D = 5$ (continuous lines).

The decrease of heat transport with the distance between wall and nozzle can be described by a power law of the type:

$$Nu = a\mathrm{e}^{-b\frac{H}{D}}. \tag{1}$$

From the simulation results, the coefficients are derived as $a = 214$ and $b = 0.26$.

The increase of the integral surface Nusselt number can be explained in terms of the inertia of the jet: for constant values of drop diameter and mass loading it can be expressed as a function of the Reynolds number as

$$Nu \propto Re^{0.8}. \tag{2}$$

This correlation is in agreement with the results available in the literature for heat transfer dynamics of impinging jets without particles (Goldstein et al., 1986). When droplets are present, due to the momentum transfer of the faster moving droplets, the gas acquires more inertia close to the wall and, as a consequence, heat transfer increases. The increase of the integral Nusselt number can be considered at first as linear with droplet diameter. Also the effect of the droplet number flux impacting the surface (Fig. 6) can be regarded as

$$Nu = Nu^{\mathrm{o}} + B\dot{n}_{\mathrm{p}}, \tag{3}$$

where Nu^{o} is the Nusselt number without droplets and B is a parameter depending on the drop diameter. The derived distribution of B is plotted in Fig. 7.

In order to evidence the importance of studying the spray also on a micro-scale, the overall heat transfer coefficient found by the simulations is compared with the experiments of Yokomine et al. (2002). These authors investigated experimentally and numerically the heat transfer mechanism during the impingement of a jet with different types of gas–solid suspensions. In the case of graphite particles suspended, a significant increase of the heat transfer coefficient with respect to single phase flow was found all over the heat transfer surface, while in the case of a glass beads suspension the heat transfer coefficient decreased compared to single phase flow. Yokomine et al. (2002) concluded that

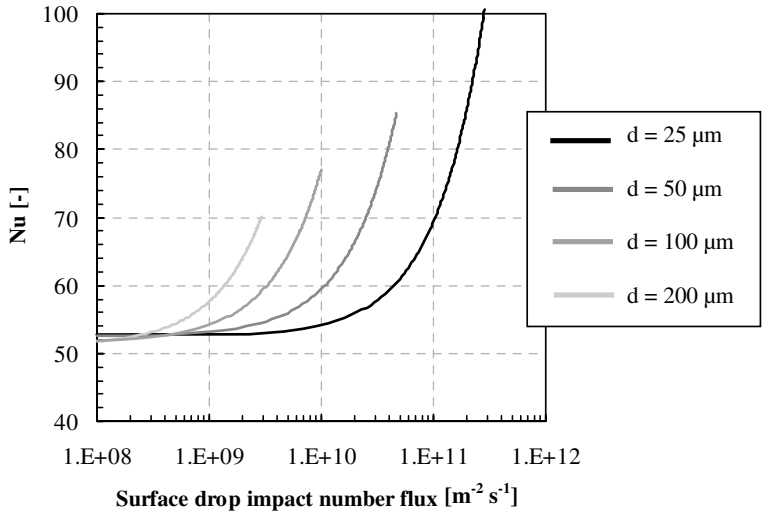

Fig. 6. Variation of the integral Nusselt number over a surface of $r/D = 1$ as function of the number of impacts per unit surface and unit of time.

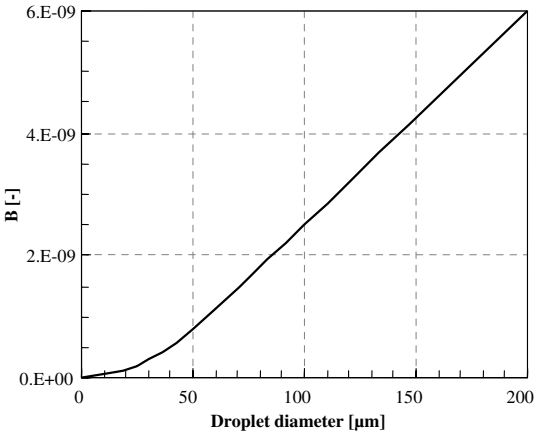

Fig. 7. Variation of the parameter B as a function of the droplet diameter.

in the case of fine and light particles like graphite, the impingement momentum of the gas phase increases because the particle incident to the boundary layer in the vicinity of the wall promotes the renewal of the boundary layer, in addition to the eddy attachment, and reduces its thickness. As a consequence, the heat transfer is enhanced more effectively. On the other side for particles with larger inertia, like glass beads, the particles rebounce or fly away from the surface acting like obstacles for the incoming gas from the nozzle, decreasing turbulence intensity and thus heat transfer.

In order to calculate heat transfer coefficients between gas and wall, one should consider in the modelling how droplets perturb the gas boundary layer close to the surface. Obviously, due to the point source assumption, the Euler–Lagrange approach does not directly take into account the influence of droplet wakes and boundary layers on the gas flow immediately at the wall and thus cannot predict in detail the droplet–surface–gas interaction that originates the increase of the heat transfer. Thus, it is necessary to study the heat transfer dynamics on the micro-scale separately and then to implement droplet effects in the adopted wall functions.

3. Micro-scale analysis

3.1. Modelling of the impact

Within the micro-scale analysis, the effect of impacting droplets on surface heat transfer has been investigated, simulating the interaction between a laminar boundary layer and perpendicularly impacting droplets. A number of influencing factors and different occurring physical phenomena are controlling the liquid drop impact as well as the gas/surface and liquid/surface heat exchange process during impact. In order to limit the number of influencing parameters for clarity of the gas/surface heat transfer investigation, some rigid boundary conditions for the impact process have been assumed.

The outcome of the impact of an individual droplet may be either deposition on the surface (spreading), fragmentation (secondary atomization into smaller droplets) with partial mass deposition, or rebouncing of the droplet. In spray deposition processes complete deposition of droplets is desired and therefore it has been assumed as the standard case for the present study. That no splashing occurs during impact for the parameters under investigation has been verified by applying the splashing criteria proposed by Mundo et al. (1998) and Bussmann et al. (2000) for droplets impacting on dry surfaces:

$$K_{\text{crit}} = We\,Oh^{-0.4} = 649 + 3.76R_D^{-0.63}. \quad (4)$$

The standard liquid in this study is a paint with Newtonian behaviour as it is used in industrial applications, its properties are given in Table 2. For this liquid properties the splashing criterion Eq. (4) is met by all droplets impacting in the present study ($K < K_{\text{crit}}$). In this investigation only the impact on dry surfaces is studied, where Cossali et al. (1997) has also given splashing limit correlation for wetted surfaces.

The spreading of a droplet during impact may be followed by its partial recoiling driven by surface tension and contact forces. The extent of recoiling is negligible if the liquid has high viscosity and low surface tension since viscosity dissipates rapidly the inertia of the droplet and the typically small surface tension does not provide enough elastic energy to retract the lamella (Rein, 1993). A liquid with these characteristics has been considered in this part of the work in order to simplify the mechanical interaction between drop and wall and to focus on heat transfer effects. Therefore, a constant value for the solid-liquid contact angle of 70° is assumed, without considering hysteresis effects for the advancing and receding liquid front (Garbero et al., 2004).

Drop impact has been simulated with the FLUENT simulation code by means of the VOF model with the geometric reconstruction scheme for the gas–liquid interphase. The VOF model adopts the concept of liquid volume fraction, whose value is unity at any point occupied by liquid and zero otherwise. In order to compute the evolution of the volume fraction field a suitable

Table 2
Droplet liquid properties

Density [kg/m^3]	1225
Viscosity [Pa s]	1.78×10^{-5}
Heat capacity [J/kg K]	1×10^{6}
Heat conductivity [W/m K]	0.6×10^{-3}
Surface tension [N/m^3]	0.03
Static contact angle [deg]	70

continuity equation is solved. The volume fraction f moves with the two fluids, in this case droplet and surrounding gas, and depends on the fluid dynamics of the whole systems that is described by the equation of conservation of mass and momentum. The liquid interphase is characterized by values of volume fraction between zero and one. The geometric reconstruction scheme (Youngs, 1982) calculates the orientation of the interface using a piecewise-linear approach. This scheme assumes that the interface between two fluids has a linear slope within each cell and uses this linear shape for calculation of the advection of fluid through the cell faces. Surface tension effects are taken into account as a body force, adding a source term in the momentum equation (Brackbill et al., 1992). The wettability of the surface is summarized by the static contact angle and results in an adjustment of the surface curvature near the wall.

A 3D-mesh composed of 300,000 cubic cells with cell size of about 20 μm has been used. The computed domain is 1.5 mm in height and includes the complete boundary layer thickness of velocity and temperature under investigation. The surface of the domain is 2 mm in width and 0.8 mm in depth, corresponding to an area of 1.6 mm^2. This size of the computational domain has been derived from sensitivity studies for evaluation of the portion of surface affected by the increment of heat transfer during the collision of a single drop.

A time step of 10^{-8} s has been adopted in all the cases. Such a small time step is required because of the large velocity difference between gas and droplet that may reduce the quality of the prediction near the interface. In order to compute the heat transfer flux between gas and surface, the total enthalpy equation from the energy balance shared among liquid and gas has been solved:

$$\frac{\partial}{\partial t}(\rho\widehat{H}) + \nabla\cdot(\rho\vec{u}\widehat{H}) = \nabla\cdot\left(\frac{k}{c_p}\nabla\widehat{H}\right). \tag{5}$$

Conduction and species diffusion terms combine to give the first term on the right hand side of the above equation. The total enthalpy per unit mass $\widehat{H}$ is defined as

$$\widehat{H} = \sum_i y_i\widehat{H}_i, \tag{6}$$

where y_i is the mass fraction of species i and $\widehat{H}_i = \int_{T_{\mathrm{ref},i}}^{T} c_{p,i}\,\mathrm{d}T + \widehat{H}_i^0(T_{\mathrm{ref},i})$. $\widehat{H}_i^0(T_{\mathrm{ref},i})$ is the enthalpy per unit mass of species i at the reference temperature $T_{\mathrm{ref},i}$. Neglecting the heat flux due to species diffusion and considering the specific heat capacity c_p independent from temperature, Eq. (5) can be written in terms of temperature:

$$\rho c_p\frac{\partial T}{\partial t} + \rho c_p\nabla\cdot(\vec{u}T) = \nabla\cdot(k\nabla T), \tag{7}$$

where the values of k, ρ, c_p depend on the local liquid volume fraction α; for instance $k = \alpha k_l + (1-\alpha)k_v$. From Eq. (7) the temperature field can be obtained in the entire computational domain.

The heat transfer coefficient is computed using Fourier's law applied to the wall:

$$h = \frac{-k\left(\frac{\partial T}{\partial n}\right)}{T_w - T_f}, \tag{8}$$

where the heat flux to the wall from a fluid cell is defined as

$$\dot{q}_w = h(T_w - T_f). \tag{9}$$

For accurate estimation of the local heat transfer coefficient in the impingement area during drop impact, the upper liquid surface after drop spreading has been considered as part of the total heat exchange surface.

3.2. Results: impact of a single droplet

In order to simulate the interaction between droplets and gas flow, velocity and temperature profiles occurring in a boundary layer flow over a flat plate at a distance of 10 cm from the beginning of the plate have been used as undisturbed gas flow and thermal fields. Two cases have been considered, with free stream gas velocity U of 20 m/s and 40 m/s corresponding to gas Reynolds numbers of 1.38×10^5 and 2.75×10^5, respectively. These values are below the laminar-turbulent transition of 5×10^5, thus indicating a laminar gas boundary layer situation. The thickness of the temperature profile is slightly larger than that of the velocity profile as the Prandtl number for the gas is 0.713. The boundary layer thickness is smaller than the height of the considered computational domain in both test cases. The maximum temperature difference between gas and wall in the test cases is again 20 K, the same as in the macro-model.

Droplets are inserted in the computational domain at a distance H of 1.1 mm above the surface and $X = 0.5$ mm downstream from the gas inlet section, as shown in Fig. 8. The droplets have a diameter $d = 200$ μm, initial velocity U_p and a direction perpendicular to the solid surface. A summary of the data regarding the used initial conditions of droplets and gas are reported in Tables 3 and 4, respectively.

A sequence of the droplet deformation and spreading process during impact of a 200 μm droplet at 10 m/s impact velocity is shown in Fig. 9. The dynamics of the droplet deformation process during impact for various boundary conditions has been correlated with existing literature data (Garbero, 2004) and shows excellent agreement.

Fig. 10 shows the dynamics of the instantaneous wall heat flow increase, related to droplet diameter and gas conductivity, averaged over the considered wall surface,

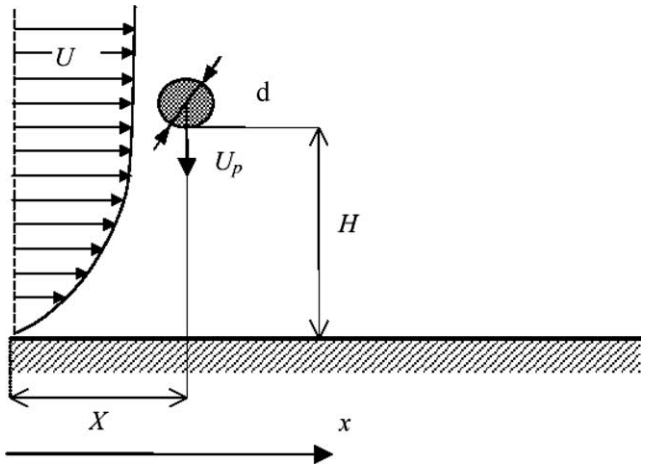

Fig. 8. Representation of the initial condition regarding the impact of a single droplet.

Table 3
Initial droplet characteristics

U_p [m/s]	Re_p	We
5	27	117
10	53	709
20	106	2835

Table 4
Initial gas flow characteristics (air)

U [m/s]	Re [–]	Pr [–]	$T_w - T_\infty$ [K]	Velocity boundary layer [mm]	Thermal boundary layer [mm]
20	1.38×10^5	0.713	20	1.3	1.44
40	2.75×10^5	0.713	20	0.95	1.01

just before drop impact in terms of $\left(\frac{\Delta \dot{Q}_w}{(T_\infty - T_w)} \frac{d}{k}\right)$, as a function of the inertial dimensionless time $\left(\tau = t \cdot \frac{U_p}{d}\right)$. By definition, the impact takes place at $\tau = 0$.

The increase of heat transfer depends on the difference of velocity magnitude between gas and droplet. The droplet acts like an obstacle to overpass for the gas flow: if it falls down at a speed much larger than the gas velocity of the undisturbed boundary layer, the gas flow underneath the droplet is displaced by the droplet to its sides and a wake may occur on top of the droplet. As a consequence, there is only a small heat flux increase at the impact surface. On the contrary, at lower droplet velocities (compared to the gas velocity of the boundary layer), the sidewise flowing boundary layer is changed and a larger amount of gas is flowing below the droplet. Here, the gas stream is more compressed in the gap between droplet and wall and as a results the temperature gradient and therefore also the heat transfer rate becomes larger.

For the same difference of velocity magnitude, the increase of heat flux is remarkably larger in the case of higher gas velocities. For low droplet impingement velocities, $U_p = 5$ m/s, the increment of heat flux before collision is sensibly larger than for the higher velocity cases. Actually, for droplet velocity of 20 m/s, the maximum increment of the heat flux is less relevant than in the other cases with lower velocities and it also affects a smaller portion of the surface. For all the cases the curves show a maximum immediately before collision at $\tau = 0$.

Fig. 11 reports the variation of heat flux after droplet impact ($\tau > 0$). The diagram shows a much larger increment in heat flux in comparison to Fig. 10, both in magnitude and in duration, due to the stronger droplet influence on velocity and temperature profile after impact.

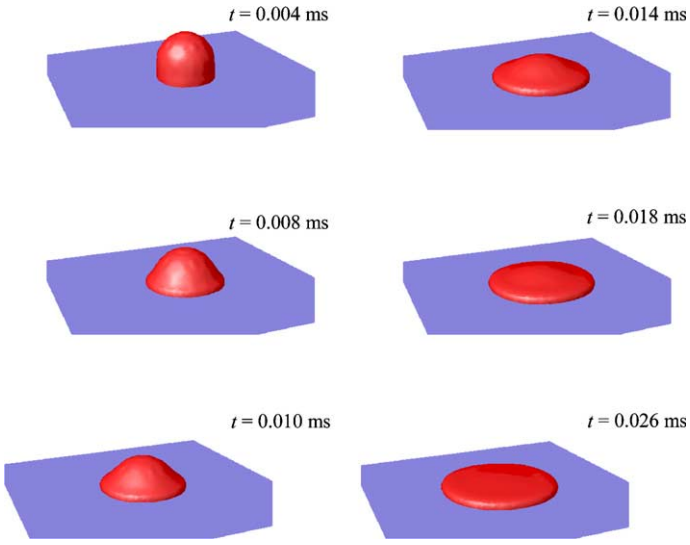

Fig. 9. Droplet deformation (spreading) during impact ($d_p = 200$ μm, $U_p = 10$ m/s).

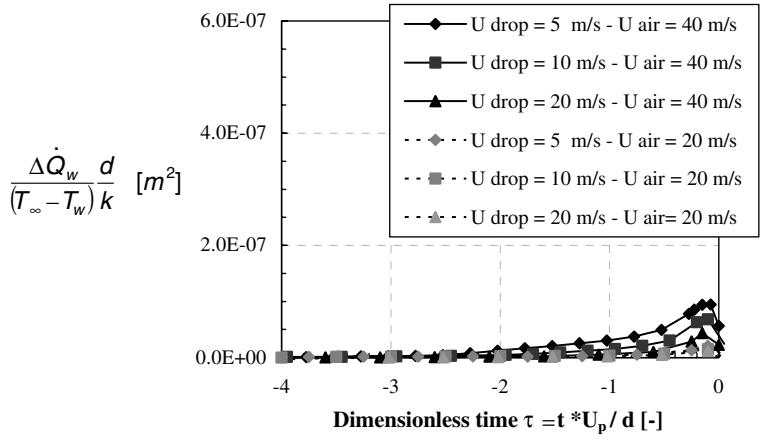

Fig. 10. Instantaneous increase of wall heat flux before impact.

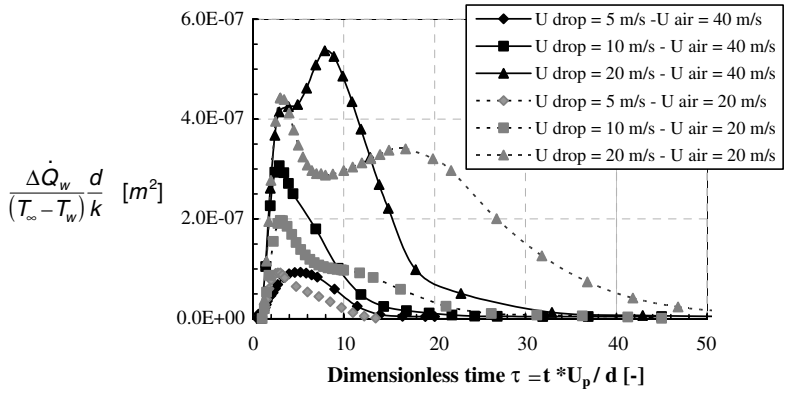

Fig. 11. Instantaneous increase of wall heat flux after impact.

The falling drop leaves a wake on its backside, which persists for some time after the impact, as highlighted in Fig. 12(a) where the instantaneous gas velocity distribution is illustrated. The gas in the wake dragged by the droplet is cooler than the gas close to the surface (Fig. 12(b): instantaneous temperature distribution) and increases the temperature gradient and therefore the local heat transfer significantly. Fig. 12(c) illustrates the heat transfer coefficient distribution on the surface and confirms this mechanism: the local increment of the heat transfer reaches a significantly larger value immediately after the spread, when the cold gas from the droplet wake reaches the surface. Subsequently the low temperature region expands on the surface under the influence of the main gas flow field. Due to this reason, in the curves of Fig. 11 at the largest impact velocity a bimodal effect is to be seen. The first maximum is due to a peak in the local heat transfer; while the second one is the result of a smaller heat flux increment spread on a larger part of the surface. Increasing the drop impact velocity, the heat flux sensibly increases and affects a larger area.

Apart from the case with impact velocity of 10 m/s and gas velocity of 40 m/s, where the maximum value of heat transfer due to the local increment and the maximum due to the effect of gas spreading occurs at the same time, the increment of heat flux in the first part of the curve is directly proportional to $Re_p^{-1.13}$.

The different duration of the phenomenon can be explained by considering the role of the droplet wake. For large difference of velocities between gas and droplet, the wake of the droplet is transported by the gas flow behind the droplet in horizontal direction, while for small difference of velocities the wake follows the droplet along the vertical direction of impact, as in Fig. 12. In this case, since the wake is aligned nearly vertically, the increase of heat transfer lasts for a longer time. On the contrary, at small impact velocity, the interaction between droplet and gas reduces the wake practically to a stagnation zone in the region not directly exposed to the gas flow. Also here some cool gas can reach the surface, but in a lower quantity and for a smaller time.

Obviously, the boundary layer profile returns to its initial condition in a short time after droplet impact and with a dynamics dependent only on the gas velocity and not on droplet speed. To be noted is the case regarding the smallest impact velocity and the maximum gas

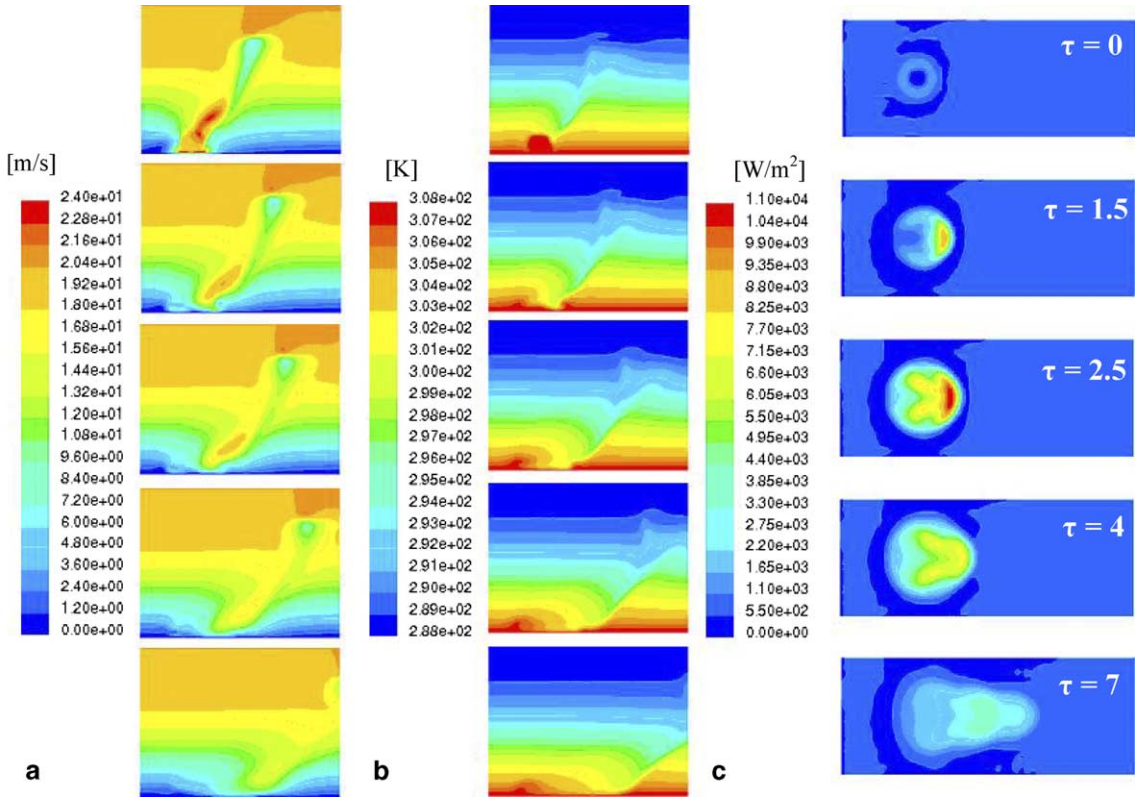

Fig. 12. Impact of a single droplet with a diameter of 200 μm, an impact velocity of 20 m/s and a maximum gas stream velocity of 20 m/s. (a) Contours of velocity (side view), (b) contours of temperature (side view), (c) contours of total surface heat flux (seen from below).

flow velocity. Here the stagnation zone interacts with the air compressed by the droplet before impact forming a stagnant gas layer on the surface. As a consequence, the gas flow takes more time to blow away the cooler gas entrapped in the wake and to reduce the increase of the heat flux. This is shown in Fig. 11, where the curve regarding the impact velocity of 5 m/s and the gas velocity of 40 m/s has the slowest behaviour compared to all the others cases.

The increment in the heat flow rate due to a single droplet disappears in an interval of time shorter than 1 ms for all the cases analysed. However, depending on the interparticle distance within a spray, the interaction between droplets needs to be considered in addition.

3.3. Results: impact of multiple droplets

So far, attention has been focussed on the study of a single droplet impact, but real sprays are composed by swarms of droplets. For example, considering a typical spray process with a liquid mass flow rate of 0.1 kg/s, at a distance of 50 cm from the nozzle, a typical figure for the number flux of particles impacting the wall per unit time is $3 \times 10^9\ \mathrm{m^{-2}\,s^{-1}}$. That is in average one impact every 0.2 ms on the previously considered surface of 1.6 $\mathrm{mm^2}$.

If the interaction among particles is neglected, one can argue that every droplet adds its contribution $\Delta\dot{Q}$ to the total heat flow transferred between gas and solid. Therefore, by time averaging the heat flow rate over a cycle of 0.2 ms, an effective heat transfer coefficient may be calculated. For example, analysing the case of drop impact velocity of 10 m/s and maximum gas velocity of 20 m/s, the effective heat transfer coefficient evaluated by this procedure assumes a value of about 43 $\mathrm{W/m^2\,K}$, as shown in Fig. 13, a value sensibly higher than that without droplets: 27 $\mathrm{W/m^2\,K}$. This evidences that also the micro-scale effect of droplets on gas–solid heat transfer needs to be considered and that not only the macro-scale influence is significant.

The results from individual droplet impacts may be regarded as an approximation, valid for dilute sprays only. Proceeding in such a way, the interaction among the wakes behind droplets is neglected, which could change the increase of heat transfer with respect to the situation computed as before. This effect could be important especially at increased droplet concentration, when the distance between particles becomes small. In order to evaluate the influence of such an interaction, three different multiple drop configurations have been simulated. Two of these regard the impact of three droplets with different initial positions, while the other one refers to a five droplet collision.

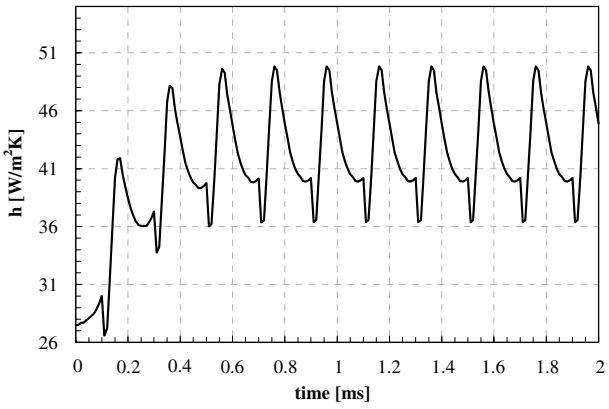

Fig. 13. Instantaneous heat transfer coefficient during the impact of a single droplet every 0.2 ms. Drop diameter = 200 μm, drop velocity = 10 m/s, maximum boundary layer velocity = 20 m/s.

The same grid configuration and computational domain as used for the single droplet case have been adopted with the target surface of 1.6 mm^2. Information about initial conditions of the droplets and of the gas profile is reported in Table 5.

The initial liquid droplet characteristics (physical properties, dimension and velocity) and the boundary layer profile of the gas are identical to those of the single droplet case with initial droplet speed of 20 m/s and maximum gas velocity of 20 m/s.

Fig. 14 exhibits the velocity vectors for the three-droplet case 1. It appears that the first two drops fall down in an undisturbed gas flow field while the last drop interacts during its motion with the wakes of the precedent two droplets. The picture shows that the wake of the left droplet covers the right one. As a consequence, the droplet on the right contrasts the circulation of the cool gas moved by the left droplet, reducing heat transfer. But the drop in the right seems also to enhance the circulation of the gas dragged by the droplet in the middle. This should result in an increase of surface heat transfer. Actually, the latter effect prevails. In order to better understand how multiple drop impacts affect the surface heat transfer, a sequence of the instantaneous heat flux exchanged at the wall (a) with the relative gas temperature profile (b) is depicted in Fig. 15, for the three-drop case 2. As it can be seen from the contours of heat flux, the first

Table 5
Initial conditions of multiple drop impact simulation

	Drop centre distance [mm]	Re_p [–]	U_p [m/s]	We [–]	Re [–]	U [m/s]	$T_w - T_\infty$ [k]
Three droplets case 1	0.79	53	20	709	1.38×10^5	20	20
Three droplets case 2	0.65						
Five droplets case	0.58						

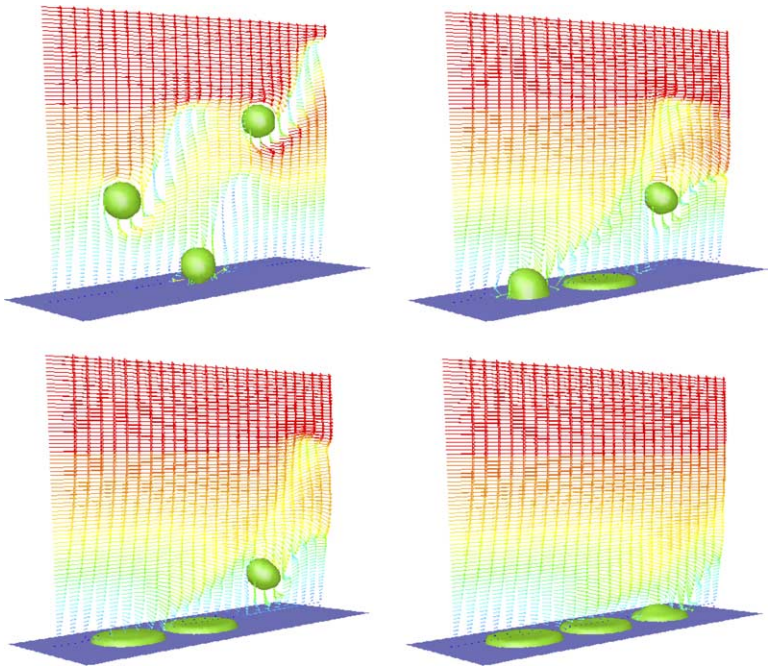

Fig. 14. Velocity vectors during the impact of three droplets: three-droplet case 1.

drop affects heat transfer in the same way as the single droplet case. The main difference appears when the other two droplets approach the surface. The second droplet acts as an obstacle for the wake of the first droplet. Indeed the moving front of cool gas dragged by the first droplet is contrasted and a stagnation zone is formed between the two formed lamellae. This reduces the area affected by the increment of heat transfer relatively to the first droplet, but makes the effect of the second droplet last longer, since in this zone the velocity of gas is lower than before. When the last droplet approaches the surface, instead, the circulation of the gas near the wall is incremented. The stagnation zone rapidly disappears and the local increment of heat transfer sensibly increases.

The simulation of the five-droplet case also confirms this dynamics. Here periodic boundary conditions have been used for gas inlet and exit sections. The effect due to the interaction between droplets is apparent in Fig. 16, where the contours of temperature at different times of impact are reported. When the first two droplets are colliding the surface, the gas flow is compressed by the droplets and bends over them. The local velocity and temperature gradients are higher and the heat flux increases in the same way as for the single droplet case. At 0.07 ms the third droplet begins to influence the gas

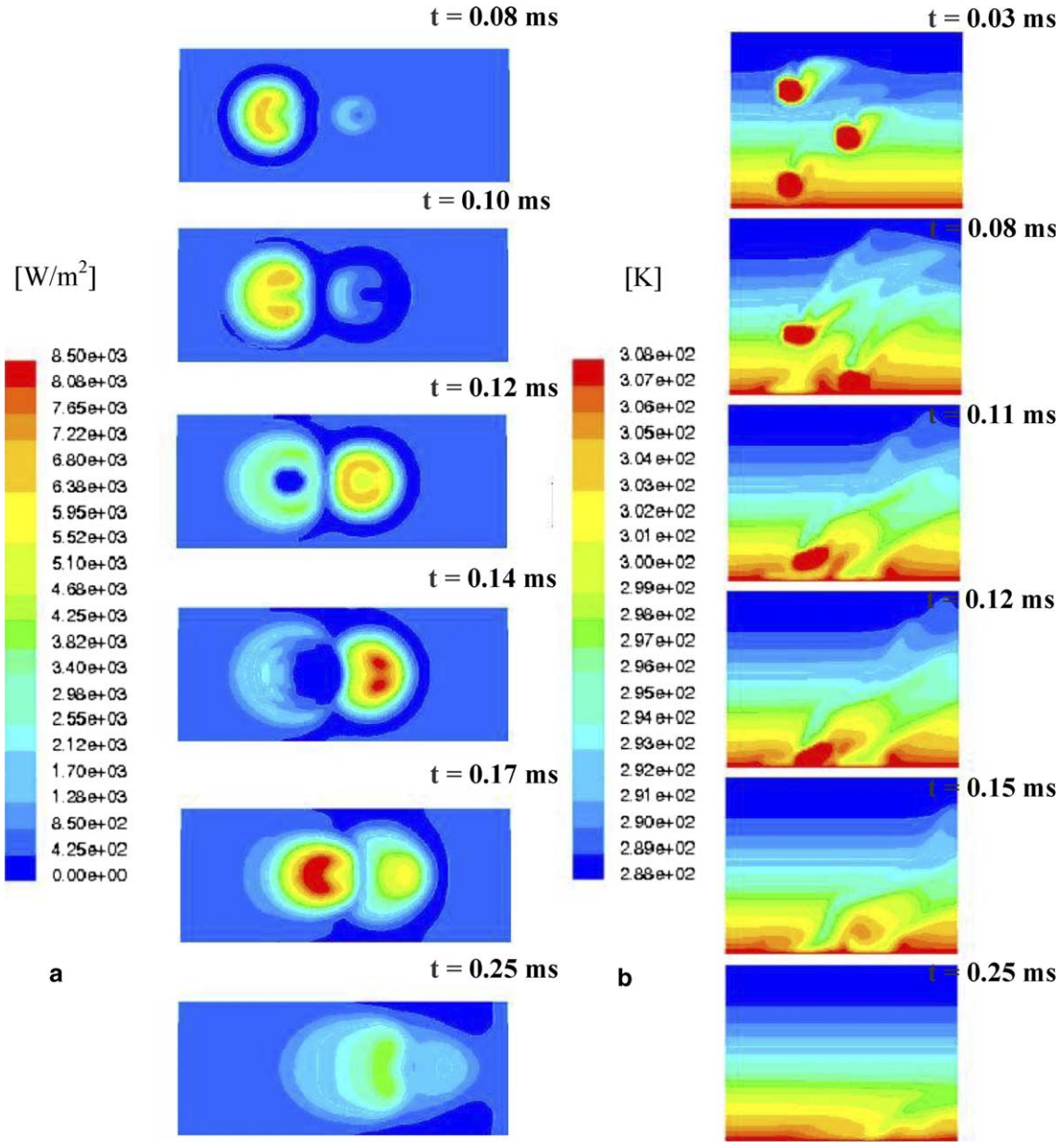

Fig. 15. (a) Contours of surface heat flux (on the left, bottom view) and (b) contours of temperature magnitude (on the right, side view). Three droplet configuration case 2.

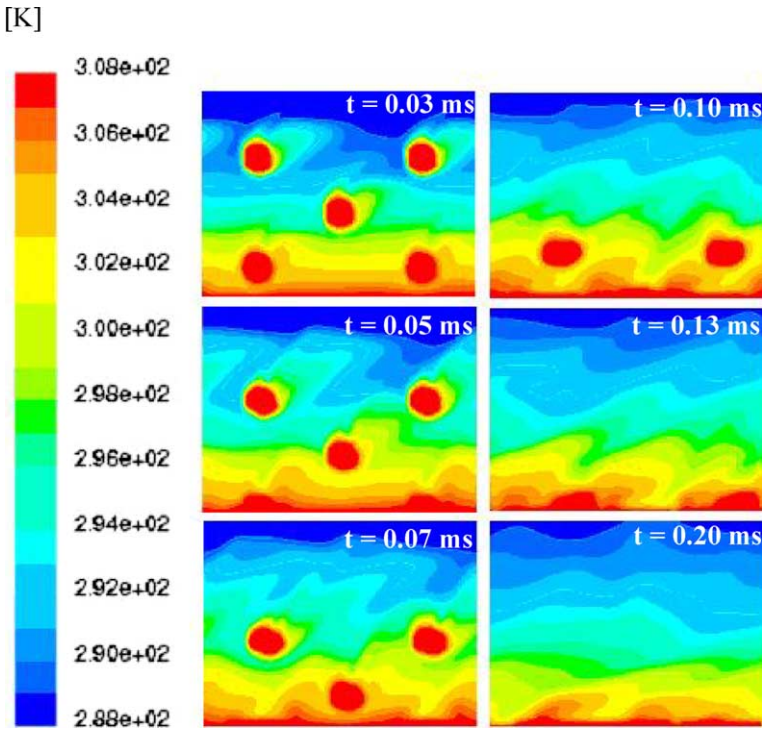

Fig. 16. Temperature contours, during the five droplet cases. Droplet diameter = 200 μm, droplet velocity = 10 m/s, maximum gas velocity = 20 m/s.

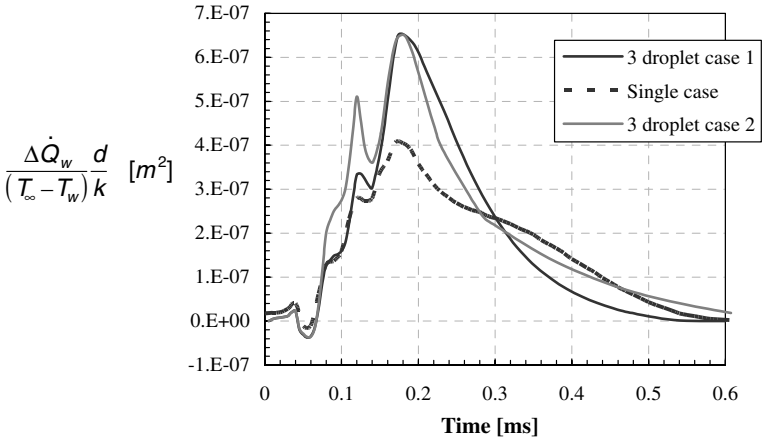

Fig. 17. Instantaneous increase of wall heat flux for the three droplet cases.

flow below it, but acts as an obstacle for the circulation of the warmer gas established by the first droplet on its left, reducing the local heat flux. When the last two droplets arrive close to the surface, the zones with small temperature are compressed between droplet and wall and a larger gas circulation is achieved. After that, the gas dragged by the last two droplets interacts with the circulation phenomena established by the other droplets, before achieving the unperturbed condition under the influence of the boundary layer gas flow.

In order to make a quantitative analysis, the increase of surface heat transfer is reported in Figs. 17 and 18 for the three and five-droplet cases, respectively. The curves indicated as "single case" have been computed summing the increase of heat flux found during the single droplet case study (no interaction between droplets is considered) for every droplet at a time correspondent to the multiple droplet case dynamics. At the beginning, all the curves present the same trend. As expected, the main difference is shown after the first impact when the second and third droplets are approaching the surface. The curves relative to the real multiple impact present similar profiles in spite of the different dynamics. This outlines that every falling droplet moving in a disturbed

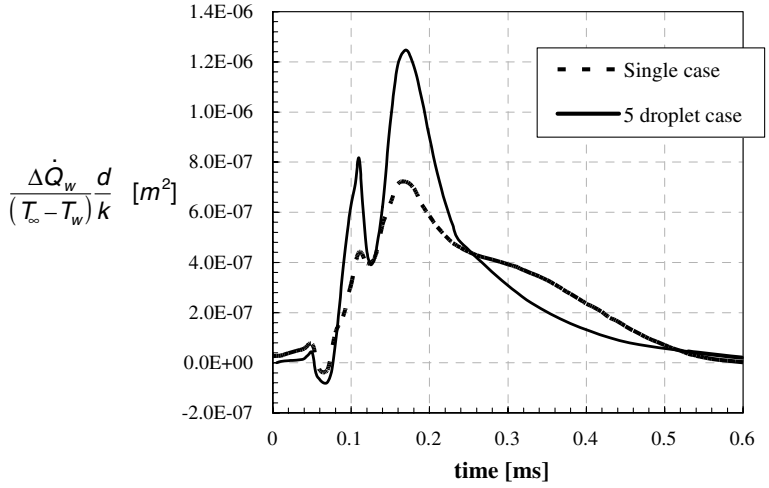

Fig. 18. Instantaneous increase of wall heat flux for the five droplet cases.

gas flow field increases heat transfer simply because a larger quantity of cooler gas from the outside is dragged towards the surface with the droplet. Actually, the second droplets, that are approaching the surface afterwards, are able to drag more cool gas to the wall due to the circulation established by the first droplets and as a consequence they increase sensibly the heat flux. The other possible interactions between wakes and droplets appear of minor importance and do not affect heat transfer significantly.

In Fig. 18, the heat transfer increase for the five-droplet case is obviously larger than for the three-droplet configuration, but the maximum increase takes again place at the same time as in the other cases. Furthermore, the magnitude of the heat transfer increase results the double of the three droplet cases. Indeed here, the number of droplets colliding the surface in the disturbed flow field can be regarded as the double of the three-droplet cases. This confirms that the further increase of heat transfer is influenced essentially by the number of droplets colliding the surface in a region where the boundary layer has been just disturbed. This makes it possible to take into account the influence on heat transfer due to multiple drop impacts by means of a further increment of the heat exchanged immediately after the collision of the second droplets. However, the increase seems of lower significance as expected. Furthermore, this increase happens only when droplets collide in a very small interval of time and onto a small area. All considerations so far have been done for droplets approaching a surface of 1.6 mm^2 and with an inter-collision time as small as 0.05 ms. This value of inter-arrival time and distance of droplets is typical for a dense spray condition where the number flux of impacting droplets is larger than $\dot{n}_p = 2 \times 10^{10}$ [$m^{-2}\,s^{-1}$]. In some applications, the time between collisions and the mean distance between droplets may be larger and the effect due to droplet and interactions are sensibly lower. For such dilute sprays, the effect of drop-drop interaction may be neglected and the results obtained during the single droplet case study are sufficient to take into account the micro-scale influence onto the gas/surface heat transfer.

4. Global effect

In this section, by expansion of the micro-scale analysis and combination with the macro-scale analysis, the overall increment of heat gas/surface transfer that takes into account the presence of droplets in a dilute spray will be derived.

The increase of the gas/wall heat transfer due to a swarm of impacting droplets, as it occurs in spray deposition, may be evaluated by multiplying the increase of exchanged heat per single droplet (reported in Figs. 11 and 12):

$$\Delta Q_w = \int_{t=0}^{\infty} \Delta\dot{Q}_w \, dt, \tag{10}$$

by the number flux $\dot{n}_p$ of particles impinging the surface per unit time and per unit surface:

$$\Delta\dot{q} = \Delta Q_w \dot{n}_p = h(T_\infty - T_w). \tag{11}$$

As an example, if the spray is generated by a nozzle of diameter $D = 5$ mm, the behaviour of the increase of the resulting Nusselt number $\left(Nu = \frac{hD}{k}\right)$ normalized by the droplet number flux for the condition adopted previously, is reported in Fig. 19. The figure confirms that for increasing the impact velocity of the droplet the heat transfer increases, but shows also a similar trend for the two curves at different boundary layer velocities. The increase of heat transfer found considering a boundary layer profile with a maximum velocity of 20 m/s is about the same order as that found for a

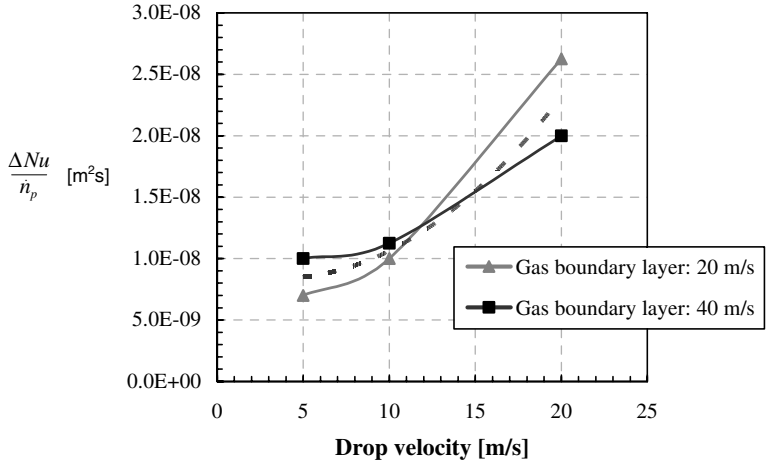

Fig. 19. Increase of local Nusselt number for a nozzle diameter of 5 mm.

boundary layer relatively of 40 m/s. Higher values of heat transfer have been found for the case with higher gas velocity, but since they are more rapidly dumped by the gas the resulting values of average during time are not so different.

Therefore, an average curve is derived to represent both cases. The dotted line in Fig. 19 represents this curve that can be correlated as

$$\frac{\Delta Nu}{\dot{n}_{\mathrm{p}}} = 5 \times 10^{-11} U_{\mathrm{p}}^2 - 4 \times 10^{-10} U_{\mathrm{p}} + 9 \times 10^{-9}. \qquad (12)$$

Fig. 20 represents the increase of Nusselt number for the impact velocities studied in the micro-scale analysis.

Finally, micro- and macro-scale effects are combined and the overall increment of the surface heat transfer can be calculated for an impinging jet or spray as a function of droplet concentration. By summing Eqs. (3) and (12), a relationship describing the global increment of Nusselt number as function of impact velocity and droplet concentration can be obtained. As an example, for droplets with diameter of 200 μm, it results in

$$Nu = Nu^{\mathrm{o}} \cdot \left[5 \times 10^{-11} U_{\mathrm{p}}^2 - 4 \times 10^{-10} U_{\mathrm{p}} + 9 \times 10^{-9}\right] \cdot \dot{n}_{\mathrm{p}} + 6 \times 10^{-9} \cdot \dot{n}_{\mathrm{p}}. \qquad (13)$$

Fig. 21 reports the overall effect of surface heat transfer due to an impinging dilute spray with an exit velocity of 20 m/s and composed by droplets of mean diameter 200 μm, colliding the surface at a velocity of 10 m/s. The figure outlines the significance of the micro-scale effect that appears even more pronounced than the macro-scale influence. Considering together micro- and macro-scale effects, the heat transfer may increase by more than 100%.

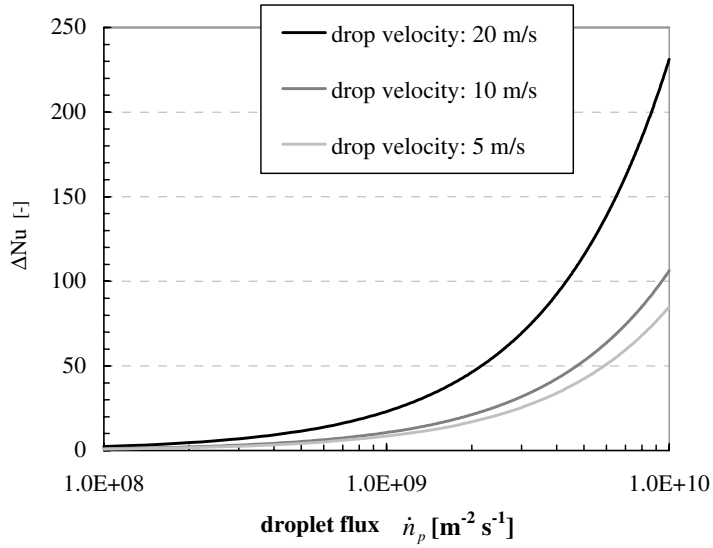

Fig. 20. Micro-scale increase of Nusselt number as a function of the droplet number flux of impinging droplets.

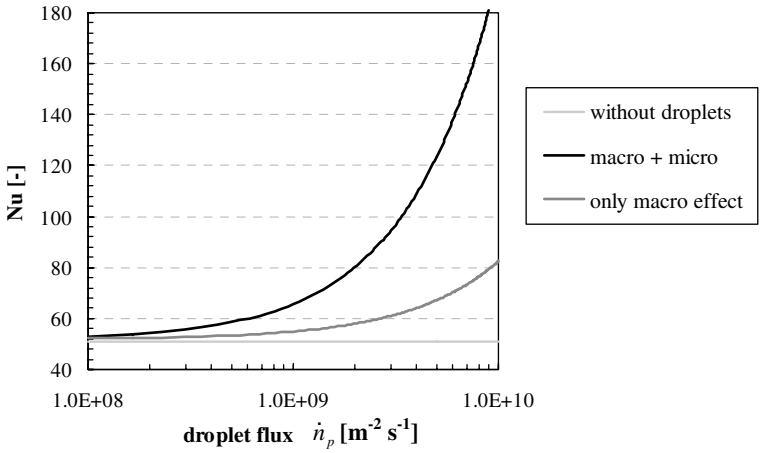

Fig. 21. Overall increase of Nusselt number during an impinging spray. Drop diameter = 200 μm, drop impact velocity = 10 m/s, jet velocity = 20 m/s.

5. Conclusions

The influence of droplet impact within spray impingement on gas/surface heat transfer has been analysed by numerical simulation from a macro- and a micro-scale point of view. Gas/surface heat transfer during spray impingement becomes important when the droplets and the surface have nearly the same temperature as, e.g., in spray coating and spray forming applications.

On the macro-scale, a two-phase jet impingement case has been studied by means of an Euler–Lagrange approach. The roles of nozzle diameter, gas velocity and nozzle/wall distance have been analysed for different values of mass loading, particle size and droplet concentration. Here, the droplets momentum transfer to the gas increases the overall jet inertia. The larger inertia creates higher velocities near the wall and increases the temperature gradients.

On a micro-scale, the fluid dynamics influence of droplet impact within a laminar boundary layer has been simulated by means of a VOF technique. The effect of the gas flow field close to the surface has been evaluated for a single-droplet impact, in order to derive the basic mechanism of the disturbance, and for the case of multiple droplet impacts, to evaluate the interaction among droplets. It has been shown that the droplets that are approaching the surface act as vortex generators, establishing a circulation of gas near the wall that increases the surface heat transfer considerably.

The study has outlined that the presence of droplets can enhance the gas/wall heat transfer considerably. The heat transfer enhancement on the macro-scale has been evaluated to about 20–40%, while that due to the micro-scale to 150%.

From these results the relevance of the perturbations of the gas boundary layer close to the surface due to the impact of droplets on heat transfer in spray application becomes obvious. Conventional prediction of the gas/surface heat transfer coefficient obtained by standard wall treatment may be inaccurate in spray applications because of its inability to describe in detail the actual surface layer of two-phase flow during spray impingement.

References

Armster, S.Q., Delplanque, J.P., Rein, M., Lavernia, E.J., 2002. Thermo-fluid mechanisms controlling droplet based material. Int. Mater. Rev. 47 (6), 265–301.

Bolle, L., Moureau, J.C., 1982. Spray cooling of hot surfaces. Multiphase Sci. Technol. 1, 1–97.

Brackbill, J.U., Kothe, D.B., Zemach, C., 1992. A continuum method for modeling surface tension. J. Comput. Phys. 100, 335–354.

Brimacombe, J.K., Agarwal, P.K., Baptista, L.A., Hibbins, S., Prabhakar, B., 1980. Spray cooling in the continuous casting of steel. In: Proc. 63rd National Open Hearth and Basic Oxygen Steel Conf., Washington, DC, pp. 235–252.

Bussmann, M., Chandra, S., Mostaghimi, J., 2000. Modeling the splashing of a droplet impacting a solid surface. Phys. Fluids 12, 3121–3132.

Butty, H., Poulikakos, D., Giannakouros, J., 2002. Three-dimensional presolidification heat transfer and fluid dynamics in molten microdroplet deposition. Int. J. Heat Fluid Flow 23, 232–241.

Chen, H.C., Patel, V.C., 1988. Near-wall turbulence models for complex flows including separation. AIAA J. 26 (6), 641–648.

Choi, K.J., Kang, B.S., 1993. Fluid mechanics and heat transfer in sprays. ASME FED, 78, HTD 270, 161–165.

Choi, K.J., Yao, S.C., 1987. Mechanisms of film boiling heat transfer of normally impacting spray. Int. J. Heat Mass Transfer 30 (2), 311–318.

Cossali, G.E., Coghe, A., Marengo, M., 1997. The impact of a single drop on a wetted slid surface. Exp. Fluids 22, 463–472.

Crowe, C.T., Sommerfeld, M., Tsuji, Y., 1997. Multiphase flows with droplets and particles. CRC Press.

Garbero, M., 2004. Modelling of spray deposition processes. Ph.D. Thesis, Politecnico di Torino, Italy.

Garbero, M., Vanni, M., Baldi, G., 2004. Analysis of drop impact onto dry surfaces. In: Proc. of the XXVII FATIPEC Congress, Aix-en-Provence, France, 19–20 April 2004.

Goldstein, R.J., Behbahani, A.I., Kieger Heppelmann, K., 1986. Streamwise distribution of the recovery factor and the local heat

transfer coefficient to an impinging circular air. Int. J. Heat Mass Transfer 29 (8), 1227–1235.
Haferl, S., Poulikakos, D., 2002. Transport and solidification phenomena in molten microdroplet pileup. J. Appl. Phys. 92 (3), 1675–1689.
Holloworth, B.R., Gero, L.R., 1985. Entrainment effects on impingement heat transfer: part II—local heat transfer measurements. ASME J. Heat Transfer 107, 910–915.
Huang, L., El-Genk, M.S., 1994. Heat transfer of an impinging jet on a flat surface. Int. J. Heat Mass Transfer 37 (13), 1915–1923.
Kader, B., 1993. Temperature and concentration profiles in fully turbulent boundary layers. Int. J. Heat Mass Transfer 24 (9), 1541–1544.
Launder, B.E., Spalding, D.B., 1974. The numerical computation of turbulent flows. Compt. Meth. Appl. Mech. Eng. 3, 269–289.
Mudawar, I., Valentine, W.S., 1989. Determination of the local quench curve for spray-cooled metallic surfaces. ASM J. Heat Treat. 7, 107–112.
Mundo, C., Sommerfeld, M., Tropea, C., 1998. On the modeling of liquid sprays impinging on surfaces. Atomization Sprays 8, 625–652.
Pasandideh-Fard, M., Bussmann, M., Chandra, S., Mostaghimi, J., 2001. Simulating droplet impact on a substrate of arbitrary shape. Atomization Sprays 11, 414–497.
Pasandideh-Fard, M., Chandra, S., Mostaghimi, J., 2002. A three-dimensional model of droplet impact and solidification. Int. J. Heat Mass Transfer 45, 2229–2242.
Rein, M., 1993. Phenomena of liquid drop impact on solid and liquid surfaces. Fluid Dyn. Res. 12, 61–93.
Rüger, M., Hohmann, S., Sommerfeld, M., Kohnen, G., 2000. Euler/Lagrange calculation of turbulent sprays: the effect of droplet collision and coalescence. Atomization Sprays 10, 47–81.
San, J.-Y., Huang, C.-H, Shu, M.-H, 1994. Impingement cooling of a confined circular air jet. Int. J. Heat Mass Transfer 40 (6), 1355–1364.
Shih, T.H., Liou, W.W., Shabbir, A., Zhu, J., 1995. A new k–ε eddy-viscosity model for high Reynolds number turbulent flows—model development and validation. Comput. Fluids 24 (3), 227–238.
Sun, J., Chen, M.M., 1998. A theoretical analysis of heat transfer due to particle impact. Int. Heat Mass Transfer 31, 969–975.
Verein Deutscher Ingenieure, 2002. VDI-Wärmeatlas, nineth ed. Springer Verlag, Berlin (Chapter Gk).
Viskanta, R., Incropera, F.P., 1992. Quenching with liquid jet impingement. Heat Mass Transfer Mater. Process., 455–476.
Yakhot, V., Orszag, S.A., 1986. Renormalization group analysis of turbulence. J. Sci. Comput. 1, 3–51.
Yokomine, T., Shimizu, A., Saitoh, A., Higa, K., 2002. Heat transfer of multiple impinging jets with gas–solid suspensions. Exp. Thermal Fluid Sci. 26, 617–626.
Youngs, D.L., 1982. Time-dependent multi-material flow with large fluid distortion. In: Morton, K.W., Baines, M.J. (Eds.), Numerical methods for fluid dynamics. Academic Press, London, UK, pp. 273–285.